Exchange coupling in Fe/NiO/Co film studied by soft x-ray resonant magnetic reflectivity

O. Zaharko*
Laboratory for Neutron Scattering, ETHZ & PSI, CH-5232 Villigen, Switzerland

P. M. Oppeneer
Institute of Solid State and Materials Research, P.O. Box 270016, D-01171 Dresden, Germany

H. Grimmer and M. Horisberger
Laboratory for Neutron Scattering, ETHZ & PSI, CH-5232 Villigen, Switzerland

H.-Ch. Mertins, D. Abramsohn, and F. Schäfers
BESSY GmbH, Albert-Einstein-Strasse 15, D-12489 Berlin, Germany

A. Bill and H.-B. Braun
Condensed Matter Theory, PSI, CH-5232 Villigen, Switzerland

A 10 nm Fe/5 nm NiO/10 nm Co polycrystalline trilayer prepared by magnetron sputtering has been investigated by resonant magnetic reflectivity of linearly polarized soft x rays (transversal magneto-optical Kerr effect geometry) at the L_3 edges of Fe, Ni, and Co. The exchange coupling in the trilayer, introduced during synthesis, has been altered by cooling through the Néel temperature T_N of NiO at three different cooling fields H_{FC}. We show that the chemical structure at the interfaces, the grain size and the magnetic properties of the trilayer are governed by factors such as successive heat treatment, magnetic field applied during synthesis and cooling through T_N of NiO. Clear evidence for oxidation of Fe and Co states has been obtained, suggestive for the formation of mixed oxides at the Fe/NiO and NiO/Co interfaces. Oxidized Fe and Co are found to carry a net magnetic moment, which couples to the moments of the metallic states. We find that the coupling between oxidized and metallic Co spins is ferromagnetic, whereas the coupling between oxidized and metallic Fe spins is antiferromagnetic. We observe the presence of two types of excess Ni spins. A rigid excess Ni magnetic moment is induced at the interface during synthesis as follows from the strong asymmetry of the x-ray Kerr loops of the oxidized Co spins at $H_{FC}=0$ Oe and metallic Co spins at $H_{FC}=240$ Oe. Heat treatment leads to appearance of a soft excess Ni magnetic moment, which is ferromagnetically coupled to the metallic Fe and Co spins and exhibits a conventional hysteresis loop. Competing interactions lead to frustrated magnetization at the NiO/Fe interface and cause a tilt of the Fe spins away from the direction of applied magnetic field. This manifests itself in the presence of characteristic humps in the Fe Kerr loops.

I. INTRODUCTION

Films composed of ferromagnetic (F) and antiferromagnetic (AF) layers play an important role in a number of applications, such as spin-valve, magnetoresistive devices, and tunnel junctions.[1–4] These devices are composed of textured and polycrystalline layers with domain size in the nanometer range. Their performance crucially depends on the chemical and magnetic structure of the AF/F interface, which determine the exchange coupling between the different layers.

In particular, the operation of such devices needs stability in certain temperature and external magnetic field intervals. Therefore, it is important to understand the influence of external conditions on the AF/F interface. It is the purpose of the present work to analyze how various factors affect the magnetic properties of multilayers and to extract information on the dominant couplings both at the interfaces and in the layers. To this aim we used soft x-ray resonant magnetic reflectivity (SXRMR) to study an exchange coupled 10 nm Co/5 nm NiO/10 nm Fe trilayer, mimicking spin-valve devices used in industry.

One of the most challenging tasks is to study the interface structure, to which end one needs to distinguish atoms of the interface and of the adjacent layers. Recent developments in synchrotron based x-ray absorption spectroscopy (XAS) and related techniques[5] allow us to tackle this problem. The XAS signal is sensitive to the chemical and magnetic states of the resonance atom. In addition, by tuning the polarization of the synchrotron light, one can study both, ferromagnetic and antiferromagnetic spin arrangements.[6–8]

Imaging techniques, such as x-ray photoemission electron microscopy (XPEEM) can be used to detect excess spins at the surface of the antiferromagnet coupled to a ferromagnetic film, and to determine the orientation of these spins. For example, XPEEM on Fe/NiO and Co/NiO bilayers[9] explicitly showed the rearrangement of the excess Ni spins at the surface of the antiferromagnetic NiO single crystal after deposition of a ferromagnetic Fe or Co film and showed that the excess Ni spins align parallel to Fe or Co spins.

Soft x-ray resonant magnetic reflectivity provides information complementing that obtained by XPEEM. A varying external magnetic field can be applied during the SXRMR measurement, so magnetization reversal of different sites of the same element can be followed. In other words, element

and state selective Kerr loops can be obtained. In addition, changing the angle of incidence alters the x-ray penetration depth, thus allowing to look deeper into the film as compared to XPEEM, where the electron escape depth is usually rather small.

The structure of the paper is as follows. In the two next sections we present the sample characterization and experimental setup. Section IV summarizes the theoretical description needed to interpret the SXRMR measurements. The identification of different electronic states of Co, Fe, and Ni is explained in Sec. V. Section VI describes the Kerr loops for each element and for three magnetic fields applied during cooling through T_N of NiO. Finally, we discuss the results in Secs. VII and VIII.

II. SAMPLE CHARACTERIZATION

A series of Co/NiO/Fe polycrystalline samples (with thicknesses 0–20 nm, Fe is the bottom layer) was produced by dc magnetron sputtering from metallic Co, Ni, and Fe targets under Ar atmosphere on a Si substrate with a base pressure of 1.7×10^{-5} mbar.[10] For the NiO layer an Ar $+ O_2$ mixture was used. Transmission electron microscopy of 10-nm-thick Fe, NiO, and Co *reference* single films showed that nanocrystalline grains of hcp/fcc Co, fcc NiO, and bcc Fe are formed with grain sizes in the range of $3-15$, $3-7$, $5-20$ nm, respectively. The chemical depth profile of the 10 nm Co/5 nm NiO/10 nm Fe trilayer has been measured by x-ray photoemission spectroscopy (XPS), which revealed diffusion of oxygen into the Fe and Co layers at the Co/NiO and NiO/Fe interfaces and partial oxidation of Co at the sample surface. Metallic Co and Fe were detected in the bulk of the layers. The interfacial mixing is expected to take place over a thickness of 2 nm, based on findings for sputtered FeNi/NiO and NiFe/oxide/Co samples.[11,12]

The magnetization of 10 nm Fe and Co single films was measured by a Quantum Design Physical Property Measurement System (PPMS) [see Fig. 1(a)]. These measurements showed that both films are soft ferromagnets with coercivities (halfwidth of the hysteresis loop) of $H_{coer} = 40$ Oe and $H_{coer} = 20$ Oe for Fe and Co, respectively. The Fe film has no preferred anisotropy in the film plane, while the Co film has an easy axis along x [the reference coordinate system defined in Fig. 2(a) is used throughout the paper]. No net moment was detected for the 10 nm NiO film. The magnetic reversal of 10 nm Co/10 nm Fe bilayer is identical to the reversal of 10 nm Fe single film [Fig. 1(b)], implying that Co and Fe magnetic domains rotate simultaneously.

Deposition of a NiO interlayer between Co and Fe layers yields a strong change of the magnetization reversal. The total hysteresis loop for the as-prepared 10 nm Co/5 nm NiO/10 nm Fe trilayer [Fig. 1(c)] is composed of two loops: a narrow one with $H_{coer} = 50$ Oe and a broad one with $H_{coer} = 250$ Oe. As is shown later, clear the narrow loop corresponds mainly to the reversal of Fe spins, while the broad loop corresponds to Co spin reversal. The Co magnetization reversal is significantly modified because the Co grains are grown on a different bottom layer as compared to the Co single film and the Co/Fe bilayer. On the other hand, the Fe
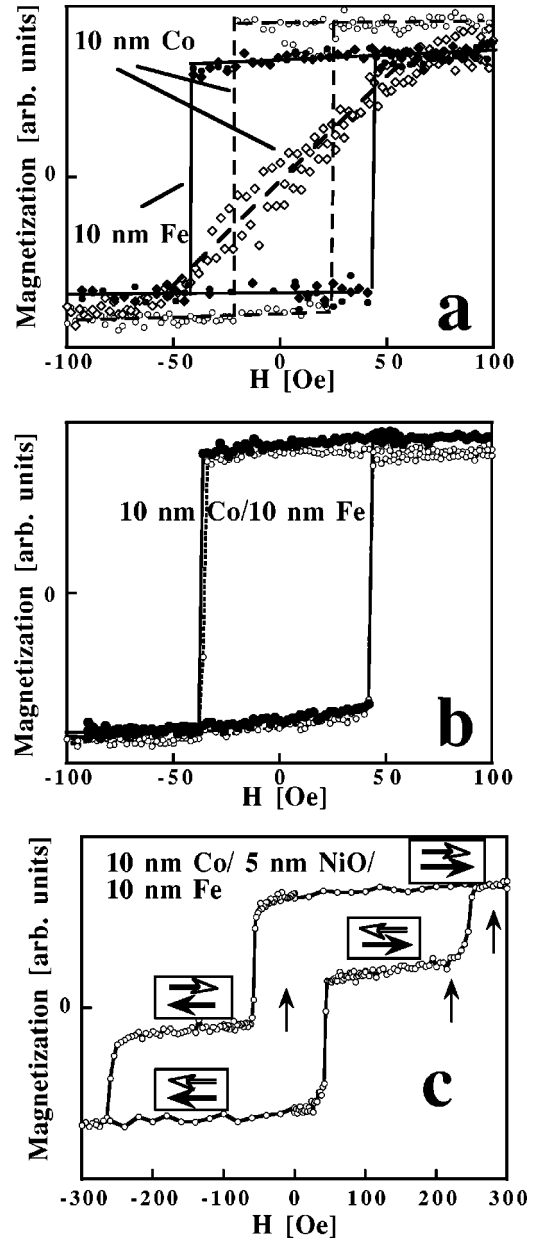
FIG. 1. The dc magnetization measured by a PPMS device for (a) 10 nm Fe and Co single films, (b) 10 nm Fe/10 nm Co bilayer, and (c) 10 nm Fe/5 nm NiO/10 nm Co trilayer. In (a), the full symbols show the Fe data and the open symbols those of Co. The circles correspond to $H\|x$ and the diamonds to $H\|y$. The reference coordinate system is defined in Fig. 2. In (b), the filled circles are the data for $H\|x$, while the open circles give the data for $H\|y$. In (c), the open arrows indicate the orientation of the majority of Co spins and the filled black arrows that of the Fe spins. The magnetic field is applied along the x axis. The three values of the cooling field are also marked.

magnetic domains are already formed when NiO is deposited and Fe magnetization reversal is less affected by NiO deposition. The presence of two loops indicates a significant decoupling of the F layers by the intercalated AF NiO layer.

To get deeper insight into the structure of interfaces and to study magnetic interactions in the trilayer we performed soft x-ray resonant magnetic reflectivity experiments.
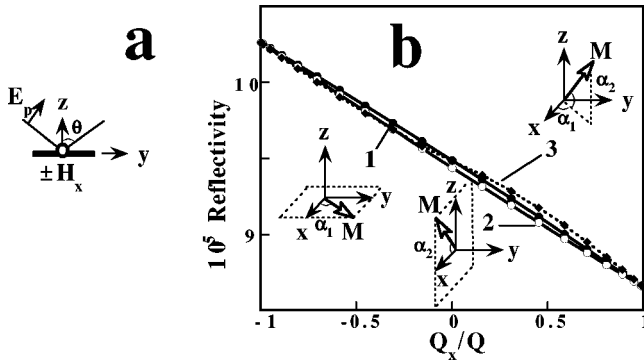
FIG. 2. (a) Reference coordinate system and T-MOKE geometry. (b) The resonant reflectivity as a function of the ratio Q_x/Q calculated for three reversal scenarios. The Fe moment rotates: in the $xy0$ plane, $\alpha_1 \neq 0$, $\alpha_2 = 0$, curve 1; in the $x0z$ plane, $\alpha_1 = 0$, $\alpha_2 \neq 0$, curve 2; in a general direction, curve 3.

III. EXPERIMENTAL SETUP

Soft x-ray resonant magnetic reflectivity of the 10 nm Co/5 nm NiO/10 nm Fe trilayer was measured at the elliptically polarizing undulator beamline UE56/1 PGM at BESSY II using the soft x-ray polarimeter.[13] The reflectivity of p-linearly polarized soft x rays was measured at the L_3 edges of Fe, Co, and Ni with external magnetic field applied within the plane of the film and perpendicular to the plane of incidence. This is the so-called transversal magneto-optical Kerr effect (T-MOKE) geometry. In the local coordinate system [see Fig. 2(a)], we choose for convenience the local x axis to be parallel to the applied magnetic field, whereas the plane of incidence is the y-z plane. The energy resolution was $E/\Delta E \approx 2580$ and the degree of linear polarization $P_L > 0.99$. The angle of incidence was fixed to $\theta_i = 70°$ from the film normal, to ensure that a sufficient reflectivity is obtained and that x rays of the resonant energy penetrate through the whole layer formed by the resonant atoms. For instance, the attenuation length at the L_3 Fe edge and the effective path through the Fe layer for $\theta_i = 70°$ are both approximately equal to 30 nm.

We modified the exchange coupling of spins at the F/AF interfaces by *in situ* heating the sample above the Néel temperature of NiO ($T_N = 230 °C$) and then cooling to room temperature. First no external magnetic field was applied during cooling $H_{FC} = 0$ Oe. Then, the sample was cooled in the presence of an external magnetic field $H_{FC} = 240$ Oe applied along the x direction. This corresponds to a plateau at the PPMS hysteresis loop [Fig. 1(c)] at which the magnetization of Fe and Co are opposite. Finally, the same procedure was repeated at $H_{FC} = 300$ Oe with Fe and Co spins aligned parallel according to the PPMS results.

No change of the nonmagnetic reflectivity across the resonance was detected for these three different states of the trilayer. This implies that there was no significant additional oxidation of the sample during successive heat treatment. Consequently, the difference in the spectra measured for $H_{FC} = 0$ Oe, $H_{FC} = 240$ Oe, and $H_{FC} = 300$ Oe can be attributed to the spatial redistribution of oxygen and to the change of the magnetic coupling of the layers.

IV. THEORETICAL FORMULATION

Soft x-ray resonant reflectivity is highly sensitive to the magnetization of the resonant atom. At the Fe, Co, and Ni $L_{2,3}$ resonances, intensive p-d multiple transitions are induced, and the corresponding magnetic reflectivity probes the magnetic electronic structure related to the d electrons.

The total resonant reflectivity contains both magnetic and nonmagnetic (i.e., charge) responses. In order to investigate the magnetic response, we consider here the variation of x-ray reflectivity as a function of applied magnetic field. In the T-MOKE geometry the external magnetic field is applied within the plane of the film, and is perpendicular to the plane of incidence. The measured reflectivity signal can be treated within the classical magneto-optical formalism,[14–16] based on the Fresnel reflection and transmission coefficients for s/p linearly polarized light. In this formalism it is customary to discuss the magnetic contribution in terms of the Voigt parameter Q, which, for a general magnetization direction is a vector, each component of $\mathbf{Q}$ being proportional to the magnetization components. In the polar Kerr geometry[15] the Voigt parameter is directly related to the dichroic parts of the refractive indices that are measured in x-ray magnetic circular dichroism (XMCD) experiments $Q\bar{n} = n_+ - n_- = 2(-\Delta\delta + i\Delta\beta)$, where $\pm$ denotes the change of the magnetization direction with respect to the helicity of circularly polarized light. The refractive indices are defined as $n_\pm = 1 - (\delta \pm \Delta\delta) + i(\beta \pm \Delta\beta)$, and $\bar{n} = 1 - \delta + i\beta$ is the average, nonmagnetic refractive index.

For an arbitrary magnetization orientation, the Fresnel reflection coefficients r_{sp} and r_{pp} that describe the coupling of an incident p-linearly polarized wave to outgoing s/p-polarized waves at an interface, are given by

$$r_{sp} = \frac{in_0\bar{n}\cos\theta_i\{Q_y\sin\theta_t - Q_z\cos\theta_t\}}{(\bar{n}\cos\theta_t + n_0\cos\theta_i)(\bar{n}\cos\theta_i + n_0\cos\theta_t)\cos\theta_t},$$

$$(1)$$

$$r_{pp} = r_{pp}^0 + \Delta_{pp} \equiv \frac{\bar{n}\cos\theta_i - n_0\cos\theta_t}{\bar{n}\cos\theta_i + n_0\cos\theta_t} + \frac{2in_0\bar{n}\cos\theta_i\sin\theta_tQ_x}{(\bar{n}\cos\theta_i + n_0\cos\theta_t)^2},$$

where n_0 is the index of refraction of the nonmagnetic transmitted medium, $\bar{n}$ the average index of the magnetic reflective medium, and θ_i and θ_t are the angles of incidence and refraction, respectively. These expressions, derived for the reflection of light from a dielectric/magnetic medium, can be directly applied to the soft-x-ray resonant reflectivity of the Fe/NiO/Co trilayer. At the L_3 resonance of a specific atom (so-called white line) its magnetic reflectivity contrast is significantly enhanced with respect to the other atoms, which can thus be treated as nonmagnetic (dielectric).

In the case of thick layers, the layer thickness exceeds the attenuation length (i.e., bulk limit) and interference effects at the following interfaces can be neglected. The measured reflectivity of p-polarized light is given by

$$R = r_{sp}r_{sp}^* + r_{pp}r_{pp}^* = R_0 + 2\text{Re}[r_{pp}^*\Delta_{pp}] + |\Delta_{pp}|^2 + |\Delta_{sp}|^2$$

$$(2)$$

which can be written as

$$R = R_0 + 2R_0 \left[\frac{\mathrm{Re}[r_{pp}^* \Delta_{pp}]}{R_0} \right] + \mathcal{O}(Q_x^2, Q_y^2, Q_y Q_z, Q_z^2), \quad (3)$$

where R_0 is the nonmagnetic reflectivity, $\mathrm{Re}[r_{pp}^* \cdot \Delta_{pp}]/R_0$ is the usual T-MOKE signal,[15] linear in Q_x. The T-MOKE part of the reflectivity gives rise to the typical, antisymmetric Kerr hysteresis loops when the magnetic field along the x direction is reversed. The third (higher order) term in Eq. (3) is much smaller and can to a good approximation be neglected in the investigation of reflectivity Kerr loops. We illustrate this in Fig. 2, where we present the calculated Kerr reflectivity at the Fe L_3 white line for three possible magnetization reversals of a metallic Fe film, assuming continuous magnetization rotation in the bulk limit. Note, that for the maximal positive (or negative) magnetic field all spins are aligned parallel (antiparallel) to the x axis and thus the ratio Q_x/Q is $1(-1)$ for all scenarios. For intermediate values of the magnetic field the reversal path may be chosen differently. For example, the Fe moment may rotate in the $xy0$ $(x0z)$ plane. Then the reflectivity will follow curve 1 (2). The reversal of the moment in a general direction would yield curve 3. As can be seen from Fig. 2, the T-MOKE reflectivity is sensitive only to the reversal of the x component of the magnetization.

In the case of thin layers (i.e., thin-film limit), the attenuation length exceeds the layer thickness, and interference effects become significant. Therefore, Eq. (3) has to be extended so as to include backscattering from the second interface. Nevertheless, due to high absorption at the Co and Fe L_3 white lines,[17–19] only 15% of the incoming x-ray intensity reaches the Co/NiO interface, and only 10% the Fe/Si interface, respectively, for our experimental geometry. X rays, reflected from either one of these interfaces, will be further absorbed propagating through the Co or Fe layers outwards of the trilayer. Therefore, we may neglect the interference at the next interfaces and use the bulk-limit description. Only at the Ni L_3 white line, 50% of the intensity reaches the NiO/Fe interface, so the thin-film limit description should be adopted in principle to analyze the data.

It can be shown, however, that the thin-film description does not alter the conclusion that for the geometry used in our experiment only the x component of the magnetization is measured. Indeed, the total reflection matrix for a film of thickness d is given by $\mathbf{R} + \exp[i2d\bar{n}\cos\theta_t(2\pi/\lambda_0)]\mathbf{R}'$ where $\mathbf{R}$ is the major (2×2) reflection matrix for the (top) dielectric/magnetic interface and $\mathbf{R}'$ the secondary reflection matrix for the (bottom) magnetic/dielectric interface. The exponential factor describes the propagation of the wave with wavelength λ_0 within the magnetic medium. It has been shown[14] that $\mathbf{R}'$ has precisely the same dependence on Q as $\mathbf{R}$. As a consequence, also in the thin-film limit the reversal of the x component of the magnetization is measured in the T-MOKE geometry.

It is known that significant inter-diffusion and oxidation/reduction of neighboring layers is possible.[11,12,20] As a result, the electronic configuration of the atoms at the interface will differ from that in the bulk of the layer. Within the magneto-optical formalism this can be described by splitting each layer into sublayers with different refractive indices n and with different magnetic (i.e., dichroic) contributions $\Delta\beta$ and $\Delta\delta$. If the dichroic contributions of these electronic states are well separated in energy, the magnetic contributions of the interface and bulk-layer states can be resolved. Thus, by choosing an appropriate energy one could measure an element- and state-specific magnetic hysteresis. However, if these dichroic contributions overlap, their fingerprints in the magnetic reflectivity contrast will be superimposed and little can be learned about the magnetism of each subsystem. As will be shown in the following sections, it is possible to resolve the contributions in our experiment.

V. IDENTIFICATION OF THE ELECTRONIC STATES OF Co, Fe, AND Ni

Figure 3 presents the measured reflectances across the Co, Fe, and Ni L_3 edges for two opposite directions of the transverse magnetic field $H_x = \pm 240$ Oe. A complex line shape is clearly present at the Co and Fe L_3 edges, which reveals the presence of atoms with different environment in the Fe and Co layers. As outlined in the previous section, a large magnetic contribution to the reflectivity is expected from those ferromagnetic states that switch magnetization direction in the applied field. For Co this occurs foremost at 777.75 eV, while for Fe it occurs at 706.8 eV. We attribute these peaks to metallic states of Co and Fe. The other peaks are identified as belonging to the oxidized states.

For the oxidized states multiplet structures are expected due to the presence of various oxidation states and local surroundings.[21] Corresponding peaks are seen for Co at 776.5 and 779.3 eV, and in Fe at 708.75 and 709.9 eV. While this is a clear indication of the presence of both metallic and oxidized states, it is more complex to identify exactly to what extent these states contribute to each peak, since the refractive indices with their dichroic contributions are not known in detail for each of these states. Nevertheless, an assignment can be made based on published x-ray absorption spectra (XAS) and XMCD data.[22] Indeed the absorptive part (β) of the refractive index is the main factor defining the reflectance profile at the chosen energies and incident angle, whereas the dichroism in absorption $(\Delta\beta)$ dominates the magnetic contrast of the reflectivity.[23] Consider first the magnetic contrast at the Co L_3 edge [Fig. 3(a)]. The maxima at 776.5, 777.75, and 779.3 eV have contributions of the multiplet structure of the oxidized Co states, as follows from the comparison with the CoO, Co_3O_4, $CoFe_2O_4$, and Co/NiO XAS spectra.[20,24–29] Metallic Co XAS contributes only to the maximum at 777.75 eV. Moreover, the XMCD asymmetry of metallic Co is maximal in the range $777.5 - 778.5$ eV,[17,19] while $\Delta\beta$ of oxidized Co is maximal in $777 - 780$ eV.[28] Thus, there is negligible overlap between $\Delta\beta$ of metallic and oxidized Co at 779.3 eV and the magnetic contrast in the reflectivity at 779.3 eV can be attributed solely to the dichroic contribution of the oxidized Co states. On account of the clear magnetic switching at 777.75 eV we can attribute this peak to metallic Co. This statement is further substantiated in Sec. VI A, where it is shown that the magnetic behavior at 777.75 eV is very different from that at 779.3 eV.
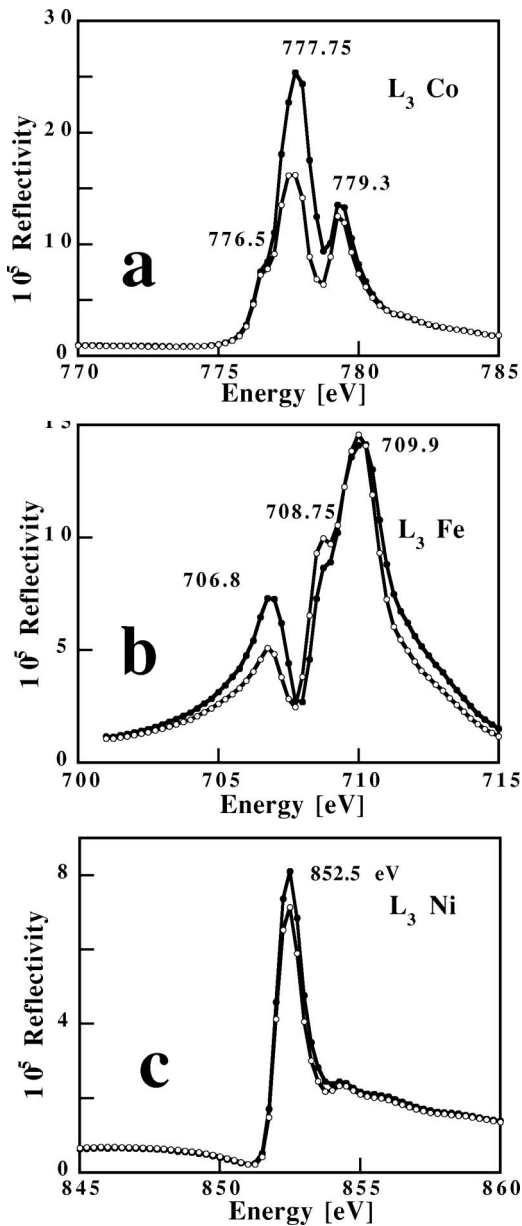
FIG. 3. The T-MOKE reflectivity at the Co (a), Fe (b), and Ni (c) L_3 edges for $\theta_i = 70°$ and $H_x = \pm 260$ Oe.

The entanglement of various states at the Fe L_3 edge [Fig. 3(b)] is more complicated than for Co. The maxima at 706.8, 708.75, and 709.9 eV have contributions of the multiplet structure of the oxidized Fe states, as follows from the comparison with FeO, α-Fe$_2$O$_3$, γ-Fe$_2$O$_3$, Fe$_3$O$_4$, Fe$_{1-x}$Ni$_x$O$_y$, and Fe/NiO XAS spectra.[20,25,30–35] The maximal absorption and XMCD asymmetry of metallic Fe is at 706.8 eV.[17,19] The contributions of FeO will appear at exactly the same energy. Therefore, metallic Fe (with possible contribution of FeO) dominates XMCD at 706.8 eV. The multiplet structures of α-Fe$_2$O$_3$ and Fe$_3$O$_4$ have a chemical shift to higher energies and their absorption maxima appear at 708.5 and 710 eV (Refs. 33, and 35) and XMCD covers $706.5 - 710$ eV range. Therefore, the magnetic contrast at 709.9 eV predominantly originates from the oxidized Fe states. Reference 33 demonstrates that the dichroism of Fe at 706.8 eV and of Fe$_3$O$_4$ at

710 eV have the same sign. As we observe a change of sign in the dichroism between 706.8 and 710 eV in Fig. 3(b), we deduce the existence of an AF coupling between metallic and oxidized Fe.

Figure 3(c) shows the Ni L_3 edge reflectivity. According to previous studies,[18,20] the energy separation of the metallic and oxidized states is nearly 0.5 eV. This energy separation is smaller than that of 1.5 in Co and 3.1 eV in Fe. It could easily be resolved within our experiment, but we do not observe any split. Moreover, the magnetic contrast appears only at the energy corresponding to the resonance of the oxidized Ni states and not at the energy where the dichroism of the metallic Ni states is expected. Therefore, we conclude that reduction of NiO at the interfaces does not lead to the formation of ferromagnetic metallic Ni, but rather to the formation of an Ni-Fe-O (or Ni-Co-O) phases in which the oxidized Ni states possess a ferromagnetic component.

VI. FIELD DEPENDENCE OF THE REFLECTANCE ACROSS THE L_3 RESONANCES

The 10 nm Co/5 nm NiO/10 nm Fe trilayer was cooled in the presence of a magnetic field $H_{FC} = 0$, 240, or 300 Oe through the Néel temperature of NiO. The reflectivity as a function of applied magnetic field was subsequently measured at the respective soft x-ray energies discussed in the preceding section. As a result, we obtain T-MOKE Kerr loops pertaining to the magnetic response of metallic and oxidized states of each element separately. We first present the experimental results for each $3d$ element and postpone their interpretation to the next section.

A. Co magnetization reversal

In Fig. 4 we show the T-MOKE magnetization loops measured for Co at 777.75 eV (metallic Co states) and 779.3 eV (oxidized Co states), for the three cooling fields. The field induced reversal of the net magnetization of both the metallic and oxidized Co states along the x direction is evident from the Kerr loops. Metallic Co spins already exhibit a ferromagnetic component at zero field and nicely follow the magnetic field. The spins of metallic and oxidized Co are aligned parallel to each other, as follows from the parallel shapes of the Kerr loops.

At $H_{FC} = 0$ Oe the hysteresis loop at 777.75 eV [Fig. 4(a), full symbols] is broad ($H_{coer} = 245$ Oe), symmetric and rounded, and no shift of the loop along the field axis (exchange bias) is observed. The magnetization reversal is governed by the formation/rotation of individual magnetic domains, and occurs in two steps. A small number of domains reverse magnetization at $H_x = \pm 120$ Oe. These steps are correlated with the reversal of the Fe spins, as will be discussed below (see Fig. 5). The majority of domains then switch at around $H_x = \pm 210$ Oe. The hysteresis loop at 779.3 eV [Fig. 4(a), open symbols] shows a different behavior: the Kerr hysteresis loop is strongly asymmetric: the positive side of the loop resembles the metallic loop shape, with somewhat higher coercivity, but on the negative field side the reversal starts already at $H_x = 0$ Oe and occurs abruptly below $H_x = -100$ Oe.
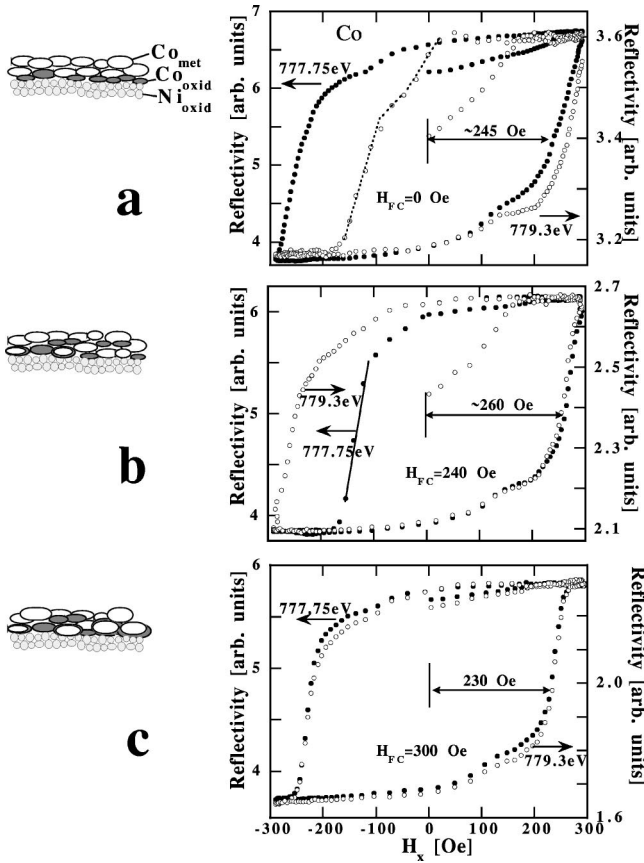
FIG. 4. Right: The reflectivity as a function of the applied magnetic field measured at the L_3 edges of oxidized (779.3 eV, open symbols) and metallic (777.75 eV, full symbols) Co states after field cooling at $H_{FC}=0$ Oe (a), $H_{FC}=240$ Oe (b), and $H_{FC}=300$ Oe (c). Changes in the Co/NiO interface due to thermal treatment are schematically depicted on the left-hand side.

After field cooling at $H_{FC}=240$ Oe [Fig. 4(b)] the magnetic reversal of oxidized and metallic Co is partially interchanged with respect to that observed for $H_{FC}=0$ Oe. The hysteresis loop at 779.3 eV (oxidized Co states) is symmetric ($H_{coer}=260$ Oe), while the loop at 777.75 eV (metallic Co states) is asymmetric: on the negative side of the loop the magnetization suddenly rotates at $H_x \approx -110$ Oe. On the positive loop side, on the other hand, the metallic and oxidized Co spins closely follow each other.

After field cooling at $H_{FC}=300$ Oe [Fig. 4(c)], the hysteresis loops at 777.75 and 779.3 eV are identically symmetric and round ($H_{coer}=230$ Oe): the oxidized and metallic Co spins reverse together.

We suggest that the origin of the observed asymmetry is exchange coupling to a rigid excess Ni magnetic moment as will be discussed below.

B. Fe magnetization reversal

The curves measured at 706.8 eV (metallic Fe states) and 709.9 eV (oxidized Fe states) are presented in Fig. 5. Since the hysteresis loops are opposite, it follows that antiparallel alignment of the spins of metallic and oxidized Fe is preferred. The resulting spin arrangement depends on the cooling field and strength of other couplings.
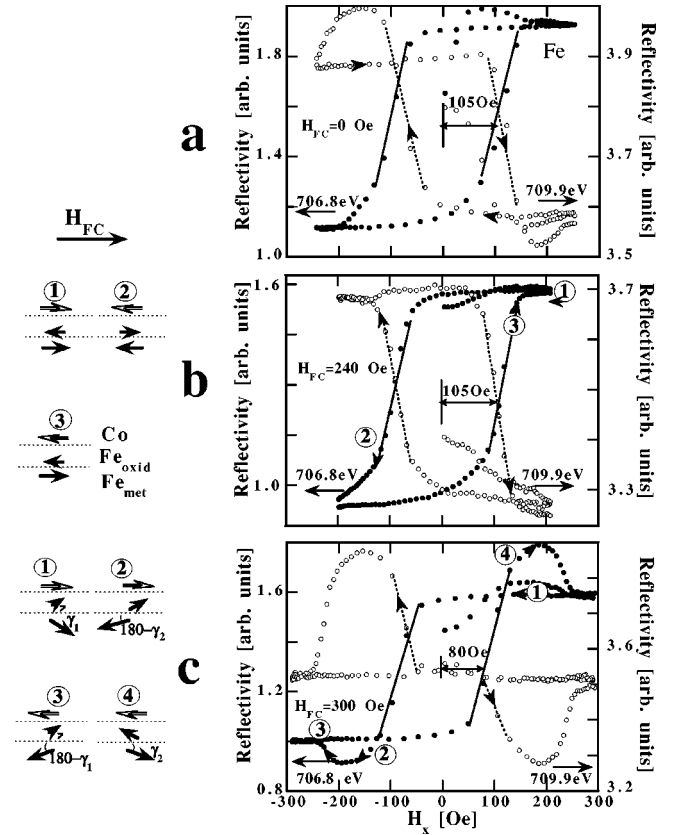
FIG. 5. Right: The reflectivity as a function of applied magnetic field measured at the L_3 edges of oxidized (709.9 eV, open symbols) and metallic (706.8 eV, full symbols) Fe states after field cooling at $H_{FC}=0$ Oe (a), $H_{FC}=240$ Oe (b), and $H_{FC}=300$ Oe (c). Left-hand side: likely arrangement of the Fe spins at various stages of the magnetization reversal.

At $H_{FC}=0$ Oe the hysteresis loop at 706.8 eV [Fig. 5(a), full symbols] is narrow ($H_{coer}=105$ Oe) and symmetric. Metallic Fe thus exhibits soft magnetic switching behavior as expected. The reflectivity at 709.9 eV (oxidized Fe states) [Fig. 5(a), open symbols] steeply decreases when $H_x > 100$ Oe, reaches its minimum value at $H_x=180$ Oe, increases again up to $H_x=240$ Oe and does not change further for higher fields. On the negative side of the loop the magnetization reverses in the opposite manner. Note the characteristic humps in the reflectivity occuring for 150 Oe $< H_x < 220$ Oe and -240 Oe $< H_x < -100$ Oe.

After field cooling at $H_{FC}=240$ Oe [Fig. 5(b)], the hysteresis loops are similar to those obtained for $H_{FC}=0$ Oe, but no humps are observed. At $H_{FC}=300$ Oe [Fig. 5(c)] the humps at 80 Oe $< H_x < 230$ Oe and -230 Oe $< H_x < -80$ Oe are significantly enhanced and the loops become narrower for both x-ray energies.

We suggest that the humps are related to a tilt of the spins of the metallic and oxidized Fe states towards/away from the x axis. This issue is addressed later on.

C. Ni magnetization reversal

The very observation of hysteresis loops measured at the Ni L_3 edge at 852.5 eV (Fig. 6) clearly indicates the presence
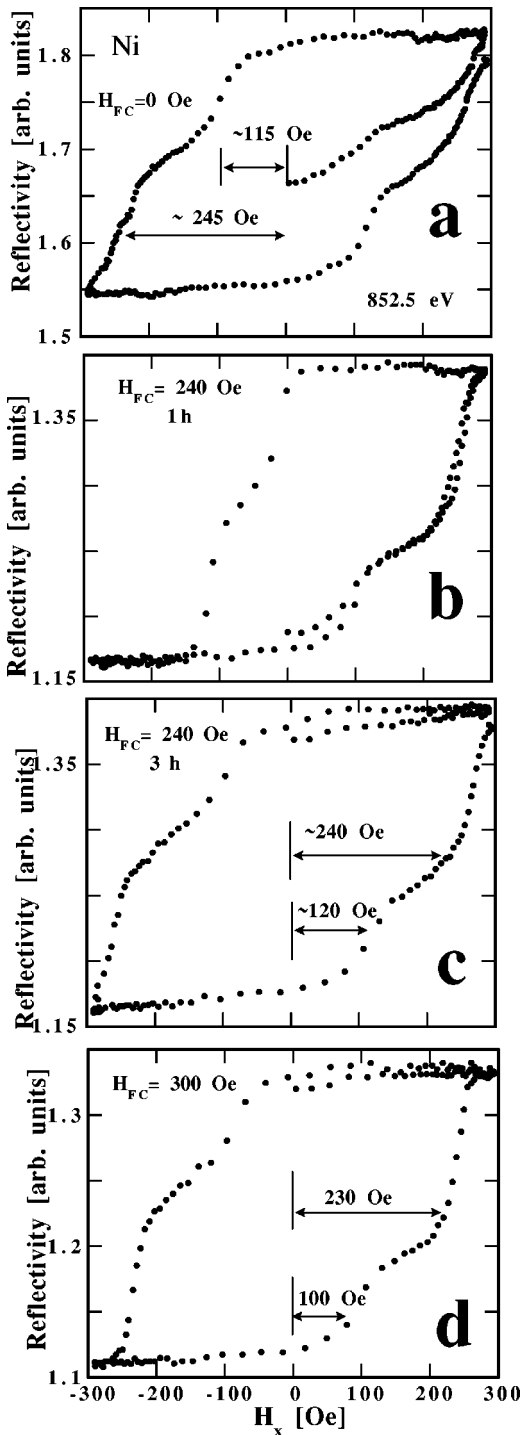
FIG. 6. The reflectivity as a function of the applied magnetic field measured at the L_3 edges of oxidized (852.5 eV) Ni states after field cooling at $H_{FC}=0$ Oe (a), $H_{FC}=240$ Oe (b), (c), and $H_{FC}=300$ Oe (d). The loops (b) and (c) were measured 1 and 3 h after the field cooling, respectively.

of an excess Ni moment, which appears after field cooling. This moment is strongly coupled to the Fe and Co spins. The reversal of the Ni spins takes place at the same field values as the reversal of Co and Fe spins, therefore, we name these Ni spins "soft." A major part of the Ni spins reverses together with Co, while a minor part with Fe. The Ni spins rotate

parallel to the majority of metallic Fe and Co spins, along the applied field direction.

Due to limited access to synchrotron light we were not able to follow the time dynamics of the exchange coupling. However, we performed two identical measurements 1 and 3 h after field cooling at $H_{FC}=240$ Oe. Interestingly, the Ni reversal changes with time: 1 hour after field cooling [Fig. 6(b)] the hysteresis loop of Ni has a similar asymmetry as the loop of metallic Co. After 3 h, the Ni loop becomes symmetric [Fig. 6(c)] while the metallic Co loop remains asymmetric. It seems that right after cooling the Ni moment is strongly coupled to metallic Co, but with time or successive magnetic reversal this coupling decreases.

It is important to note here that findings at the Co L_3 edge suggest the existence of a rigid excess Ni magnetic moment, as will be discussed later. However, the direct observation at the Ni L_3 edge is not possible. This is because in the performed experiment we did not change the polarization of soft x rays, but only altered the applied magnetic field H_x. In addition, the magnitude of H_x was too small to rotate the rigid excess Ni spins.

VII. DISCUSSION

The present SXRMR study of the Co/NiO/Fe trilayer indicates oxidation of Fe and Co at the Co/NiO and NiO/Fe interfaces. The entangled profile of the reflectivity at the Fe, Co L_3 edges reminds, in addition to metallic Fe and Co, the rich multiplet structure of Fe and Co oxides. In bulk binary oxides this multiplet structure originates from Co^{2+}, Co^{3+}, Fe^{3+}, and Fe^{2+} ions occupying octahedral and tetrahedral sites. Our observations thus indicate that complex $Fe_{1-x}Ni_xO_y$ and $Co_{1-x}Ni_xO_y$ mixtures form at the interfaces, with Co and Fe ions having several oxidation states, symmetries and environments. The oxidation at the interfaces originates from the magnetron sputtering of the trilayer, which is often accompanied by diffusion of sputtered atoms into adjacent layers. The interdiffusion is of the order of 2 nm at each interface. The top of the Fe layer may have been oxidized during the reactive sputtering of Ni. It should be noted that oxidation of metallic layers was reported also for samples prepared by other methods: MO/M bilayers (MO = NiO, CoO and M = Co, Fe, or Ni) produced by molecular beam epitaxy[20] and for an ion beam sputtered NiO/FeNi bilayer.[11] Additional diffusion of oxygen may occur at 330 K (Ref. 36) or during subsequent heat treatments of the sample. As we already mentioned, however, no significant change in reflectivity at the oxidized/metallic states resonances was observed. This implies that the amount of oxidized/metallic states stays approximately the same. Nevertheless, our findings suggest spatial redistribution of the oxidized/metallic states (grain motion, etc.).

An essential result of our study is that the oxidation of Fe and Co strongly affects the magnetic properties of the system. The oxidized states possess significant net magnetic moments, which couple to the magnetic moments in adjacent metallic layers. This leads to formation of a rather complex magnetic system with various competing exchange interactions that change with heat treatment and field cooling.

A. NiO magnetic behavior

Let us first analyze the magnetic behavior of the antiferromagnetic NiO layer. It is evident from the Kerr loops that after cooling through the Néel temperature of NiO an excess Ni moment appears even at $H_{FC} = 0$ Oe (Fig. 6). It couples ferromagnetically to metallic Fe and to all Co spins. This is consistent with the XMCD results on an Fe/NiO bilayer[37] and the XPEEM study of Fe/NiO and Co/NiO bilayers.[9] However, in our case the observed excess Ni moment is soft in the sense that the coupling to ferromagnetic metallic Fe and Co domains dominates over that to AF NiO grains.

Our data also suggest the existence of an additional excess Ni moment, rigidly coupled to AF grains. The indications come from the Co spin reversal (see below). This rigid Ni moment exists at the Co/NiO interface and has a component opposite to the x direction that is most likely induced by the magnetic field applied during the magnetron sputtering. This moment is not modified significantly by H_{FC}. This is due to a preferred in-plane orientation of grains with the hard axis aligned along H_{FC}. As antiferromagnetic NiO has pronounced magnetic anisotropy [$K_{\perp 111} \approx 10^4 K_{\parallel 111}$ (Ref. 38)], the magnetic field applied during cooling from T_N of NiO is too small to align NiO AF domains and rigid Ni moment along H_{FC}. Usually magnetic fields above 1 kOe are needed.[8,37,38]

B. Co magnetic behavior

The existence of an asymmetry in the Co magnetization reversal without visible shift of the Kerr loop indicates that the Co magnetization reversal is governed by two different mechanisms at the two sides of the loop and possibly nucleates at different locations in the layer. It seems that the reversal initiates at the Co/NiO interface, when H_x decreases from 300 Oe, and at the top of the Co layer, when starting from negative $H_x = -300$ Oe. Such asymmetric reversal was visualized for Co/NiO (Ref. 39) and NiFe/FeMn (Ref. 40) bilayers by imaging techniques. The images revealed the asymmetric formation of the nucleation centers depending on the sign of the applied field.

As reported above, we observe significant asymmetry in the magnetization reversal of the oxidized Co at $H_{FC} = 0$ Oe and metallic Co spins at $H_{FC} = 240$ Oe, while the asymmetry is absent at $H_{FC} = 300$ Oe. The following picture may describe these observations.

(i) An asymmetry in the oxidized Co reversal [Fig. 4(a)] is induced during sample growth and/or during the first heating/cooling cycle at $H_{FC} = 0$ Oe. In this state an oxidized Co layer has formed at the Co/NiO interface and oxidized Co spins exchange couple to the rigid excess Ni moment. When starting from positive H_x the interfacial oxidized Co spins flip at almost 0 Oe, mainly triggered by the additional field caused by the rigid excess Ni moment. This creates a domain wall in the Co layer, which moves up to the surface. When starting from negative H_x the surface or bulk metallic Co domains rotate first, drawing subsequently the interfacial Co oxidized spins in the magnetization reversal (overcoming thereby the coupling to the rigid excess Ni spins).

(ii) The asymmetry in the metallic Co loop [Fig. 4(b)] is induced by field cooling at $H_{FC} = 240$ Oe. It appears at the negative side of the loop, in the direction of the Co magnetic moment during field cooling. It is important to note [see Fig. 1(c)] that, contrary to the case $H_{FC} = 0$ where the magnetization of Fe and Co (metallic) are parallel to each other, at $H_{FC} = 240$ Oe Fe and Co have antiparallel magnetization. The starting magnetization configuration is thus different after the two FC. To understand that the hysteresis loop of the metal rather than of the oxidized state is now asymmetric we suggest that second heating/cooling cycle leads to a redistribution of oxygen away from the interface into the bulk of the Co layer. Metallic Co grains are then in direct contact with the rigid excess Ni moment, which is not modified significantly by H_{FC}. This exchange coupling between metallic Co/ rigid Ni leads to the observed asymmetry.

(iii) The absence of the asymmetry in the Co reversal at $H_{FC} = 300$ Oe [Fig. 4(c)] is caused by the increase of the Co grain size. The increase of the grain size with successive heat treatments leads to larger ferromagnetic domains, a fact corroborated by the decrease of the coercivity with heat treatment. The change of H_{coer} is most pronounced between the $H_{FC} = 240$ Oe and $H_{FC} = 300$ Oe experiments [Figs. 4(b), 4(c)]. From above considerations it is expected that at $H_{FC} = 300$ Oe [Fig. 4(c)] ferromagnetic Co domains are large enough to couple to several NiO grains with different orientations of the Neel vector. A strongly reduced exchange coupling results from the averaging over grains.

C. Fe magnetic behavior

Let us now turn to the analysis of the Fe spins. No significant asymmetry is observed in their hysteresis loop. This points towards the fact that the AF/F exchange coupling at the NiO/Fe interface is too weak to pin the Fe spins. Instead, we find that metallic Fe/oxidized Fe moments are coupled strongly. This coupling is antiferromagnetic ($J_{metFe/oxFe} < 0$), similar to the antiparallel coupling observed in Fe_3O_4/Fe and FeO/Fe systems.[33,41] During field cooling this AF $J_{metFe/oxFe}$ coupling and an effective magnetic field, composed of the cooling field and the field induced by the net magnetic moments of other atoms (for example, Co), dictate the arrangement of the Fe spins.

During the $H_{FC} = 240$ Oe field cooling the effective magnetic field felt by the oxidized Fe spins is small, as H_{FC} applied along the x direction is small and Co moments are aligned opposite to the field. The dominant $J_{metFe/oxFe}$ coupling governs the antiparallel alignment of the metallic and oxidized Fe spins along x during the whole measured Kerr loop [Fig. 5(b), states 1–3].

After the $H_{FC} = 300$ Oe field cooling the effective magnetic field acting on the oxidized Fe spins is enhanced, as H_{FC} is larger and Co moments are aligned along the field. The energy of the $J_{metFe/oxFe}$ interaction and the Zeeman energy become comparable. This leads to a magnetic frustrated state in which the Fe magnetic moments tilt away from the x axis. This tilt is reflected in the characteristic humps observed in Fig. 5. According to these observations the following magnetic configurations are identified along the hyster-

esis loop when field cooling at $H_{FC} = 300$ Oe. We start with the configuration of state 1 [Fig. 5(c)]: the metallic Fe spins tilt away from the x direction by an angle γ_1 and oxidized Fe spins align perpendicular to the field. The tilt of the metallic Fe spins occurs because of a simultaneous coupling to the oxidized Fe spins $\perp x$ and to the magnetic field $\parallel x$. The magnetization reversal of such a frustrated initial state is rather complex. At $H_x < -50$ Oe, the metallic Fe spins start rotating towards the field to reach the angle $180 - \gamma_2$ [Fig. 5(c), point 2]. Because of the $J_{metFe/oxFe}$ interaction, the oxidized Fe spins rotate into the opposite direction. At $H_x < -200$ Oe the rotation of Co spins along the field increases the effective magnetic field on the frustrated oxidized Fe spins and they align again $\perp H_x$ [Fig. 5(c), point 3]. Simultaneously, the AF $J_{metFe/oxFe}$ interaction forces metallic Fe spins to tilt away from the $-x$ direction and to adopt the tilt angle $180 - \gamma_1$.

Note that when the tilt angle is γ_2 or $180 - \gamma_2$, the T-MOKE signal of the Fe metallic spins is large. For the tilt angles γ_1 and $180 - \gamma_1$ the T-MOKE signal is smaller. This implies that $\gamma_1 > \gamma_2$ leading to characteristic humps in the Kerr loop.

The Kerr loop of the oxidized Fe spins can be described in a similar way, but the tilt angle is different. The tilt angle must be 90° at points 1 and 3 of Fig. 5(c) as the Kerr signal is the same for a maximal field of $H_x = 300$ Oe and for $H_x = 0$ Oe.

Our observations suggest that the magnetization reversal of the Fe and Co states is correlated. Presumably this exchange coupling between Fe and Co states is mediated by the NiO layer.

Another possible explanation for the observed humps of Fig. 5 has also been considered. The Kerr loop may be decomposed into two elemental loops. Such a pair is depicted in Fig. 7(a). The sum of the loops I and II yields a hysteresis curve similar to the reflectivity curve of metallic Fe shown in Fig. 5(c). In Fig. 7(b) two more elemental loops, III and IV, are presented; their sum resembles the reflectivity curve of oxidized Fe. It should be noted, however, that while this hypothesis could explain the findings at 706.8 eV it fails to explain satisfactorily the findings of the oxidized state at 709.9 eV. Indeed, at 706.8 eV there could be a major contribution of the metallic Fe (narrow part of the loop) and a minor contribution of another oxidized Fe state, which has a bonding environment typical for FeO (broad part of the loop). At 709.9 eV the narrow loop is dominant and opposite to H. Since the XMCD of metallic Fe is negligible at this energy, this narrow loop cannot originate from that metallic Fe state. We would have to assume the existence of an oxidized Fe state, responsible for the narrow part of the loop. This second oxidized state should be coupled to metallic Fe, but the direction of its magnetization rotation should be opposite to metallic Fe and the applied magnetic field. The minor broad loop belongs to the other oxidized Fe state which can be the state contributing to the broad loop at 706.8 eV. The latter assumption furthermore requires that the peaks at 706.8 and 709.9 eV have reversed contrast. This is quite unlikely as for Fe_3O_4 and FeO the sign of XMCD features is
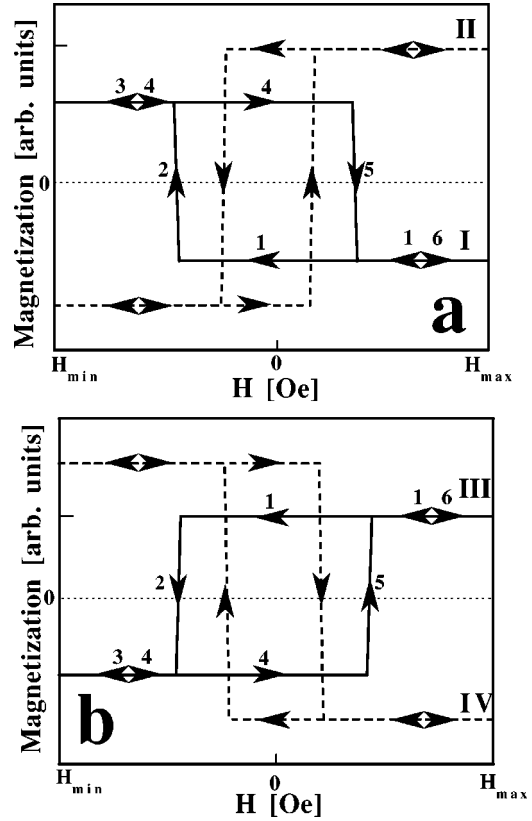
FIG. 7. Elemental loops (a), (b) reproducing the humps observed for the Fe magnetization reversal. Numbers 1–3 and 4–6 follow the magnetization reversal, when the applied magnetic field decreases from H_{max} to H_{min} and then increases from H_{min} to H_{max}.

the same at these energies.[33] In addition, if several oxidized states existed, they should also contribute at the intermediate cooling field $H_{FC} = 240$ Oe. But the Kerr loops at this H_{FC} are rather conventional and do not require the assumption of two different elemental loops. On the basis of these considerations, we are confident that the first explanation of the humps (tilting of the Fe spins away from the applied magnetic field axis) is the relevant one for the system studied.

VIII. SUMMARY

We have shown that soft x-ray magnetic resonant reflectivity gives unique information on the chemical structure and magnetic exchange interactions in a 10 nm Co/5 nm NiO/10 nm Fe trilayer. It was possible to observe and separate the magnetic contributions of the metallic and oxidized states using the shift in energy of the resonances and the differences in the shape of the T-MOKE Kerr loops.

We studied how heat treatment and magnetic field applied during cooling changes the microstructure and exchange couplings of metallic and oxidized states of different layers in the trilayer. Our findings lead to the conclusion that much care has to be taken in the synthesis of trilayer structures implemented in present applications (such as spin valves). In

particular, the chemical composition of the interface and the grain size crucially determine the magnetic properties of the trilayer. The use of polycrystalline oxides leads to unconventional hysteresis loops, which are controlled by the diffusion of oxygen in the system and change of grain size during growth and successive heat treatments. These affect in an essential way interface properties and therefore also the magnetic behavior of multilayers. Our work shows that further systematic studies of F/AF and F/F interfaces are essential to fully understand the rich physics contained in bilayer and trilayer nanomagnetic materials.

*Email address: Oksana.Zaharko@psi.ch

[1] J. Nogués and I.K. Schuller, J. Magn. Magn. Mater. **192**, 203 (1999).

[2] A.E. Berkowitz and K. Takano, J. Magn. Magn. Mater. **200**, 552 (1999).

[3] M.D. Stiles and R.D. McMichael, Phys. Rev. B **59**, 3722 (1999).

[4] P. Miltényi, M. Gierlings, J. Keller, B. Beschoten, G. Güntherodt, U. Nowak, and K.D. Usadel, Phys. Rev. Lett. **84**, 4224 (2000).

[5] J.B. Kortright, D.D. Awschalom, J. Stöhr, S.D. Bader, Y.U. Idzerda, S.S.P. Parkin, I.K. Schuller, and H.-C. Siegmann, J. Magn. Magn. Mater. **207**, 7 (1999).

[6] C.T. Chen, Y.U. Idzerda, H.-J. Lin, G. Meigs, A. Chaiken, G.A. Prinz, and G.H. Ho, Phys. Rev. B **48**, 642 (1993).

[7] V. Chakarian, Y.U. Idzerda, H.-J. Lin, C. Gutierrez, G.A. Prinz, G. Meigs, and C.T. Chen, Phys. Rev. B **53**, 11 313 (1996).

[8] W. Zhu, L. Seve, R. Sears, B. Sinkovic, and S.S.P. Parkin, Phys. Rev. Lett. **86**, 5389 (2001).

[9] H. Ohldag, A. Scholl, F. Nolting, S. Anders, F.U. Hillebrecht, and J. Stöhr, Phys. Rev. Lett. **86**, 2878 (2001).

[10] During magnetron sputtering a magnetic field is applied to the targets, this results in 20–30 Oe at the sample position.

[11] Q.Y. Xu, G. Ni, H. Sang, and Y.W. Du, J. Phys.: Condens. Matter **13**, 5047 (2001).

[12] T.S. Plaskett, P.P. Freitas, N.P. Barradas, M.F. da Silva, and J.C. Soares, J. Appl. Phys. **76**, 6104 (1994).

[13] F. Schäfers, H.-Ch. Mertins, A. Gaupp, W. Gudat, M. Mertin, I. Packe, F. Schmolla, S. di Fonzo, G. Soullié, W. Jark, R. Walker, X. le Cann, R. Nyholm, and M. Eriksson, Appl. Opt. **38**, 4074 (1999).

[14] Z.J. Jang and M.R. Scheinfein, J. Appl. Phys. **74**, 6810 (1993).

[15] P. M. Oppeneer, *Magneto-Optical Kerr Spectra*, in *Handbook of Magnetic Materials*, edited by K. H. J. Buschow (Elsevier, Amsterdam, 2001), Vol. 13, pp. 229–422.

[16] J.B. Kortright and S.-K. Kim, Phys. Rev. B **62**, 12 216 (2000).

[17] C.T. Chen, Y.U. Idzerda, H.-J. Lin, N.V. Smith, G. Meigs, E. Chaban, G.H. Ho, E. Pellegrin, and F. Sette, Phys. Rev. Lett. **75**, 152 (1995).

[18] C.T. Chen, F. Sette, Y. Ma, and S. Modesti, Phys. Rev. B **42**, 7262 (1990).

[19] Data from our reference films.

[20] T.J. Regan, H. Ohldag, C. Stamm, F. Nolting, J. Lüning, J. Stöhr, and R.L. White, Phys. Rev. B **64**, 214422 (2001).

[21] F.M.F. de Groot, J. Electron Spectrosc. Relat. Phenom. **67**, 529 (1994).

[22] To bring different experiments to the same energy scale, the pronounced features of the multiplet structure were used.

[23] Modeling of the SXRMR with/without dichroic contributions $\Delta\beta$ and $\Delta\delta$ shows that the magnetic contrast vanishes for $\Delta\beta=0$, while no significant change was observed for $\Delta\delta=0$.

[24] F.M.F. de Groot, M. Abbate, J. van Elp, G.A. Sawatzky, Y.J. Ma, C.T. Chen, and F. Sette, J. Phys.: Condens. Matter **5**, 2277 (1993).

[25] T. Jo and T. Shishidou, J. Phys. Soc. Jpn. **67**, 2505 (1998).

[26] K. Okada and A. Kotani, J. Phys. Soc. Jpn. **61**, 449 (1992).

[27] D. Bazin, P. Parent, C. Laffon, O. Ducreux, J. Lynch, I. Kovacs, L. Guszi, and F.M.F. de Groot, J. Synchrotron Radiat. **6**, 430 (1999).

[28] F. Sette, C.T. Chen, Y. Ma, S. Modesti, and N.V. Smith, in *X-ray and Inner-shell Processes*, edited by T. Carlson *et al.*, AIP Conf. Proc No. 215 (AIP, Woodbury NY, 1990), p. 787.

[29] L. Seve, W. Zhu, B. Sinkovic, J.W. Freeland, I. Coulthard, W.J. Antel, Jr., and S.S.P. Parkin, Europhys. Lett. **55**, 439 (2001).

[30] J.P. Crocombette, M. Pollak, F. Jollet, N. Thromat, and M. Gautier-Soyer, Phys. Rev. B **52**, 3143 (1995).

[31] J.H. Paterson and O.L. Krivanek, Ultramicroscopy **32**, 319 (1990).

[32] X. Wang, F. de Groot, and S.P. Cramer, J. Electron Spectrosc. Relat. Phenom. **78**, 337 (1996).

[33] H.-J. Kim, J.-H. Park, and E. Vescovo, Phys. Rev. B **61**, 15 284 (2000).

[34] C.L. Chang, G. Chern, C.L. Chen, H.H. Hsieh, C.L. Dong, W.F. Pong, C.H. Chao, H.C. Chien, and S.L. Chang, Solid State Commun. **109**, 599 (1999).

[35] P. Kuiper, B.G. Searle, P. Rudolf, L.H. Tjeng, and C.T. Chen, Phys. Rev. Lett. **70**, 1549 (1993).

[36] C.R. Brundle, Surf. Sci. **66**, 581 (1977).

[37] A.D. Alvarenga, F. Garcia, L.C. Sampaio, C. Giles, F. Yokaichiya, C.A. Achete, R.A. Simão, and A.P. Guimarães, J. Magn. Magn. Mater. **233**, 74 (2001).

[38] M. Fraune, U. Rüdiger, G. Güntherodt, S. Cardoso, and P. Freitas, Appl. Phys. Lett. **77**, 3815 (2000).

[39] H.D. Chopra, D.X. Yang, P.J. Chen, H.J. Brown, L.J. Swartzendruber, and W.F. Egelhoff, Jr., Phys. Rev. B **61**, 15 312 (2000).

[40] V.I. Nikitenko, V.S. Gornakov, A.J. Shapiro, R.D. Shull, K. Liu, S.M. Zhou, and C.L. Chien, Phys. Rev. Lett. **84**, 765 (2000).

[41] K. Koike and T. Furukawa, Phys. Rev. Lett. **77**, 3921 (1996).